

Effect of High Order Phonon Scattering on the Thermal Conductivity and Its Response to Strain of a Penta-NiN₂ Sheet

Chenxin Zhang, Jie Sun, Yiheng Shen, Wei Kang, and Qian Wang*

Cite This: *J. Phys. Chem. Lett.* 2022, 13, 5734–5741

Read Online

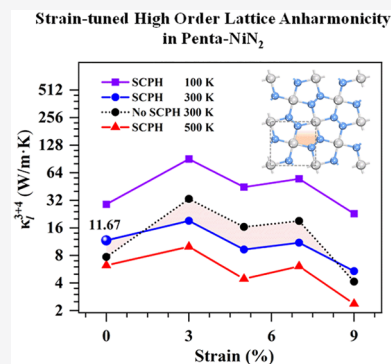
ACCESS |

Metrics & More

Article Recommendations

Supporting Information

ABSTRACT: Motivated by the recent synthesis of penta-NiN₂, a new two-dimensional (2D) planar material entirely composed of pentagons [*ACS Nano* 2021, 15, 13539], we study its thermal transport properties based on first-principles calculations and solving the Boltzmann transport equation within the self-consistent phonon theory and four-phonon scattering formalism. We find that the intrinsic lattice thermal conductivity of penta-NiN₂ is 11.67 W/mK at room temperature, which is reduced by 89.32% as compared to the value obtained by only considering three-phonon scattering processes. More interestingly, different from the general response of thermal conductivity to external strain in most 2D materials, an oscillatory decrease of the thermal conductivity with increasing biaxial tensile strain is observed, which can be attributed to the renormalization of vibrational frequencies and the nonmonotonic variation of phonon scattering rates. This work provides an accurate intrinsic thermal conductivity of penta-NiN₂ and elucidates the effects of the strain-tuned vibrational modes and phonon band gap on the four-phonon scattering processes, shedding light on a better understanding of the physical mechanisms of thermal transport properties in 2D pentagon-based materials.



Strain-tuned High Order Lattice Anharmonicity in Penta-NiN₂

Although great advances in anharmonic lattice dynamics have been made, a comprehensive understanding of the thermal transport properties of 2D materials remains challenging because the effects of temperature on the strong anharmonicity and the role of high order phonon scattering processes were usually ignored in previous studies.^{1–6} To obtain more accurate thermal conductivity, four-phonon scattering theory and self-consistent phonon (SCPH) renormalization need to be introduced into the calculations for analyzing the effects of temperature and high order lattice anharmonicity on lattice thermal transport properties.^{7–10} For instance, in 2018, Tadano et al.¹¹ studied the lattice thermal conductivity of Ba₈Ga₁₆Ge₃₀ and its thermal response to strain based on the SCPH calculation, and they found that the hardening of rattling modes induced by the high order anharmonicity significantly affects the calculated values of the lattice thermal conductivity. Feng et al.⁷ found that the calculated lattice thermal conductivity of naturally occurring Si matched better with the experimental values when four-phonon scattering was included. They demonstrated the significance of four-phonon scattering in studying the lattice thermal conductivities of diamond and graphene.¹² In particular, Kang et al.¹³ solved the problem of the disagreement between the experimental and calculated thermal conductivities of boron arsenide by using the three- and four-phonon scattering theories. In addition, thermal conductivity is a key factor that determines the thermal transport properties of a material, while most previous studies on 2D thermal materials have only considered three-phonon scattering for their thermal conductivities,^{14–19} which usually leads to

overestimation. Recently, Sun et al.²⁰ studied the thermal conductivity of 2D SnSe in the paraelectric phase by using the SCPH theory combined with high order phonon scattering, and they found that the thermal transport properties of such 2D materials can only be correctly described by using the SCPH theory and four-phonon scattering. These theoretical calculations have achieved good agreement with experimental results, indicating the necessity of using the SCPH theory and high order lattice anharmonicity in the calculations of thermal conductivity.

In general, phonon scattering strongly depends on the geometric configuration and interatomic bonding of a material. From this point of view, 2D pentagonal sheets²¹ provide a unique platform for studying phonon scattering due to their special geometries where the structural units are irregular pentagons rather than regular hexagons as in graphene. As a result, the lattice thermal conductivity κ_l of pentagonal 2D materials exhibits very different characteristics from those of conventional 2D materials. For instance, the κ_l of pentagraphene (PG)²² was found to be about 645 W/mK at room temperature,²³ which is significantly reduced as compared to that of graphene, and to show a weak dependence on the

Received: May 20, 2022

Accepted: June 16, 2022

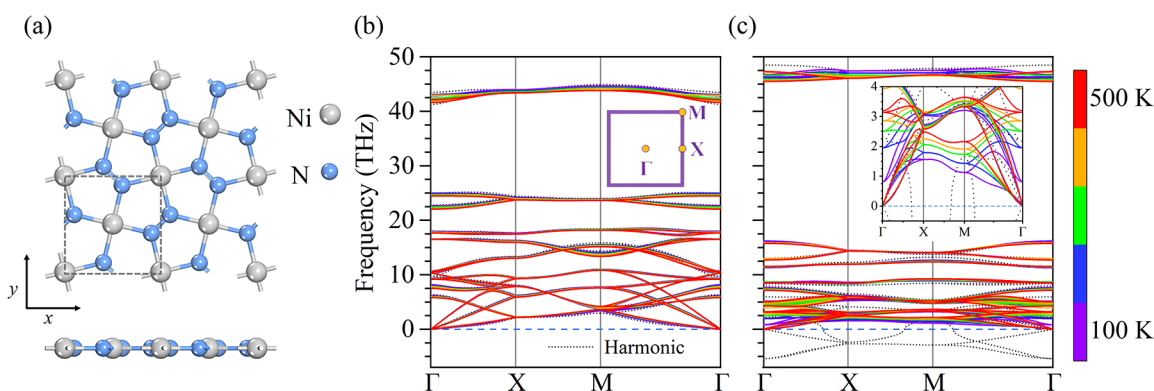


Figure 1. (a) Top and side views of the geometric structure. (b and c) Phonon spectra of penta-NiN₂ with 0% and 13% biaxial strain at different temperatures (100–500 K). The inserts in parts b and c show the Brillouin zone with the high symmetry points and the phonon branches below 4 THz, respectively, where gray dotted lines represent the phonon spectra calculated without SCPH renormalization.

stacking thickness for stacked PG sheets,²⁴ in sharp contrast to graphene, due to the strong phonon scattering in PG induced by its hybrid *sp*² and *sp*³ bonding nature and buckled structure, while the κ_l of penta-SiC₂ exhibits an unusual nonmonotonic up-and-down behavior with tensile strain and that of stretched penta-SiN₂ has 1 order of magnitude enhancement due to the strain induced buckled to planar structure transition.²⁵ Such exotic features and novel properties of penta-sheets motivate us to explore their thermal transport and phonon scattering mechanisms.

Recently, a new pentagonal 2D sheet, penta-NiN₂, was successfully synthesized by a combination of crystal-chemical design and high pressure synthesis.²⁶ It is an atomic-thick planar sheet composed of Ni₂N₃ pentagons, forming a Cairo-type mosaic, and is a direct band gap semiconductor with promising applications in nanoelectronics.²⁷ However, due to the complexity and high computational cost, no study has been reported yet for the effect of strain-tuned four-phonon scattering processes on the lattice thermal conductivities of pentagonal 2D materials. For the penta-NiN₂ sheet, there are two features that induce high order phonon scattering: (1) the large mass difference between Ni and N atoms and (2) the complex chemical bonding hierarchy, i.e. weak Ni–N bonding vs strong N–N bonding. In this work, we study the intrinsic lattice thermal conductivity of penta-NiN₂ and its thermal response to biaxial tensile strain via solving the Boltzmann transport equation (BTE) by considering four-phonon scattering combined with the SCPH theory, and we further illustrate the mechanisms of SCPH renormalization and strain-tuned high order phonon scattering in penta-NiN₂.

Our calculations are based on density functional theory (DFT) with the projector-augmented wave method (PAW)^{28,29} implemented in the Vienna *ab initio* simulation package (VASP).³⁰ The electronic exchange–correlation interaction is treated by using the Perdew–Burke–Ernzerhof functional (PBE)³¹ within the generalized gradient approximation (GGA).³² The Heyd–Scuseria–Ernzerhof hybrid functional (HSE06)^{33,34} is used to obtain the accurate band structure. The kinetic energy cutoff for the wave function is set to 520 eV. The Brillouin zone is represented with a 11 × 11 × 1 Gamma-centered *k*-point mesh for geometry optimization. The convergence criteria for energy and force are set as 10^{−8} eV and 10^{−6} eV/Å, respectively. A vacuum space of 16.00 Å in the direction perpendicular to the sheet is used to make the 2D structure free of interactions with its periodic images.

The microscopy description of κ_l can be derived from the phonon Boltzmann transport equation³⁵ within the three-phonon and four-phonon scattering frameworks. The intrinsic κ_l of an infinite and isotropic single layer can be expressed as follows:

$$\kappa_l^{\alpha\beta} = \frac{1}{k_B T^2 \Omega N} \sum_{\lambda} f_0 (f_0 + 1) (\hbar \omega_{\lambda})^2 v_{\lambda}^{\alpha} v_{\lambda}^{\beta} \tau_{\lambda} \quad (1)$$

where α and β are the directions of the Cartesian coordinate system, λ is the phonon mode consisting of wave vector and phonon branch indexes, k_B is the Boltzmann constant, T is the absolute temperature, Ω is the volume of the unit cell, N is the number of discrete q points in the Brillouin zone, f_0 is the Bose–Einstein distribution statistics, \hbar is the reduced Planck constant, ω_{λ} is the frequency of each phonon mode, v_{λ} is the phonon group velocity, and τ_{λ} is the phonon lifetime (relaxation time). The calculations of thermal conductivity and phonon properties can be solved by the ShengBTE package.³⁶

The inputs for the calculations of lattice thermal conductivity are harmonic (second-order) and anharmonic (third- and fourth-order) interatomic force constants (IFCs). For penta-NiN₂ with 4 × 4 × 1 supercell and 3 × 3 × 1 *k*-point meshes, the phonon dispersion relationship and eigenvectors are calculated by PHONOPY using the finite displacement method.³⁷ The structures for the calculations of third-order and fourth-order IFCs are generated using the random displacement method implemented in the HIPHIVE package.³⁸ The second-order IFCs considering the temperature effects based on the SCPH theory are obtained by training the data using the HIPHIVE package.^{38,39} For the second-order IFCs, the cutoff distance is taken to be 9.50 Å. For the third-order and fourth-order IFCs, the cutoff distances 6.00 and 5.00 Å, are used, respectively. In solving the Boltzmann transport equation for phonons, *q*-point meshes of 161 × 161 × 1 and 21 × 21 × 1, respectively, are adopted for the calculations of κ_l^3 and κ_l^{3+4} , while the scalebroad parameter of 0.1 is chosen. The thickness of vacuum space for the calculations of lattice thermal conductivity is set to 6.80 Å, which is obtained by calculating the sum of the upper and lower van der Waals (vdW) radii.^{40,41} The convergence tests are conducted as shown in Figure S1 in the Supporting Information.

The crystal structure of penta-NiN₂ is shown in Figure 1a, which has a perfect planar configuration with the symmetry *P4/mbm* and contains two Ni and four N atoms in its unit cell

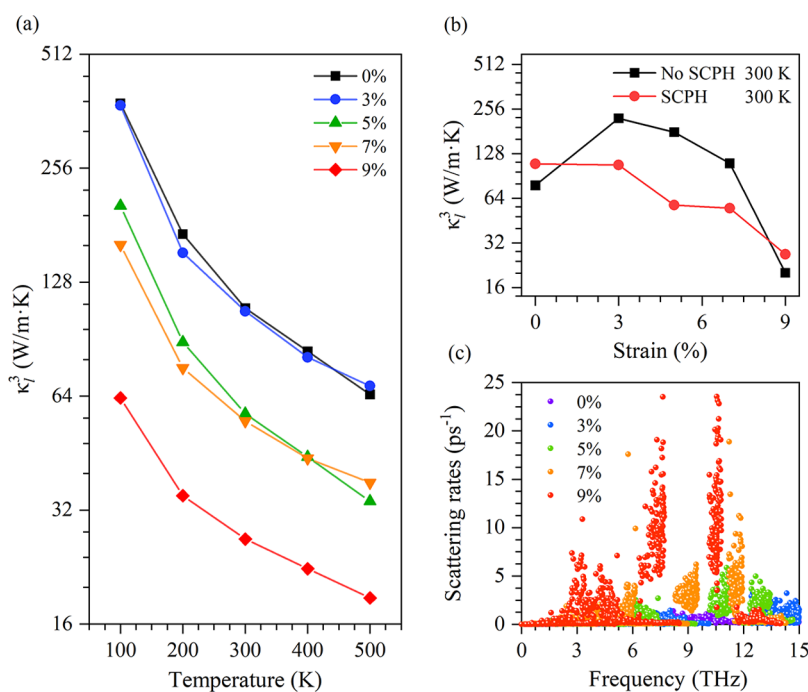


Figure 2. (a) Variation of the lattice thermal conductivity κ_l^3 with temperature for penta-NiN₂ sheets with and without tensile strain along the x direction. (b) Change of κ_l^3 with strain at 300 K calculated with and without the SCPH. (c) Change of the three-phonon scattering rates with vibrational frequencies below 15 THz under different strain conditions at 300 K.

marked with dashed lines. Our calculated lattice parameters are 4.53 Å along the x and y directions, and the bond lengths of the Ni–N and N–N bonds are 1.88 and 1.24 Å, respectively, which are consistent with previous calculated results.²⁷

To examine the stability of penta-NiN₂, we first calculate its phonon spectrum and plot the results in Figure 1b, which shows no imaginary frequencies in the entire Brillouin zone, confirming that penta-NiN₂ is dynamically stable. Meanwhile, we carry out the *ab initio* molecular dynamics (AIMD) simulations, calculate the elastic constants, and find that penta-NiN₂ is also thermally stable at high temperatures up to 1000 K and mechanically stable because the total potential energy remains almost constant during the simulations and no obvious geometric distortion is observed, as shown in Figure S2, and the elastic constants fully satisfy the Born–Huang elastic stability criteria ($C_{11} > |C_{12}|$ and $C_{66} > 0$)^{42–44} (see Table S1). The results are in good agreement with those of the previous study,²⁷ verifying the reliability of our calculations.

We also study the dynamical stability of penta-NiN₂ under biaxial tensile strain. We find that the imaginary frequencies do not arise until 9% tensile strain is applied; namely, penta-NiN₂ is dynamically unstable under a tensile strain over 9% within the harmonic approximation theory due to the existence of imaginary modes, as shown in Figure S3. However, it can be dynamically stable until 13% tensile strain when considering the SCPH, as shown in Figure 1c, implying that the resistance of some 2D materials to tensile strain might be underestimated due to the limitation of the methods used in previous studies.^{25,45}

Based on the analysis of stability, we further calculate the band structure of penta-NiN₂ at the HSE06^{33,34} level. The result is plotted in Figure S4a, which shows the semi-conducting feature with a direct band gap of 1.10 eV, consistent with the previous study,²⁷ further validating the accuracy of our calculations. According to the calculated

phonon spectra and band structures, the thermal conductivity of penta-NiN₂ can be considered to be mainly attributed to phonon transport. Therefore, we investigate the lattice thermal conductivity and the detailed mechanisms of the phonon transport behaviors of this newly synthesized 2D pentagonal sheet.

The lattice thermal conductivity κ_l^3 of penta-NiN₂ is calculated via the BTE theory by considering three-phonon scattering processes and SCPH renormalization. The change of κ_l^3 with temperature in the range from 100 to 500 K is plotted in Figure 2a, exhibiting the expected temperature (T) dependence of a $1/T$ downward trend, similar to most 2D materials. The intrinsic lattice thermal conductivity is 109.25 W/mK at 300 K. We note that our calculated thermal conductivity is much lower than the value of 610 W/mK as reported by Mortazavi et al.⁴⁶ This difference may originate from the choice of vacuum layer thickness and the inaccuracy of their used machine learning potential as discussed.⁴⁷ In addition, it is understandable that the κ_l^3 of penta-NiN₂ is much lower than those of PG (645 W/mK)²³ and penta-CN₂ (660 W/mK)⁴⁸ because penta-NiN₂ has a significantly higher average mass as compared to PG and penta-CN₂ sheets.

In practical application, a monolayer sheet cannot be free-standing. When 2D materials are placed on some substrates, strain usually exists due to external forces or lattice mismatch.⁴⁹ Furthermore, strain engineering as an effective strategy has been used to adjust the electronic, optical, and thermal transport properties of 2D materials.^{49,50} Therefore, it is important to study the thermal response of a new 2D material to external strain. We then analyze the thermal response of penta-NiN₂ to biaxial tensile strain for a deep understanding of its thermal transport properties.

One can see in Figure 2b that the response of thermal conductivity to strain calculated by using the second-order IFCs without SCPH renormalization is consistent with the

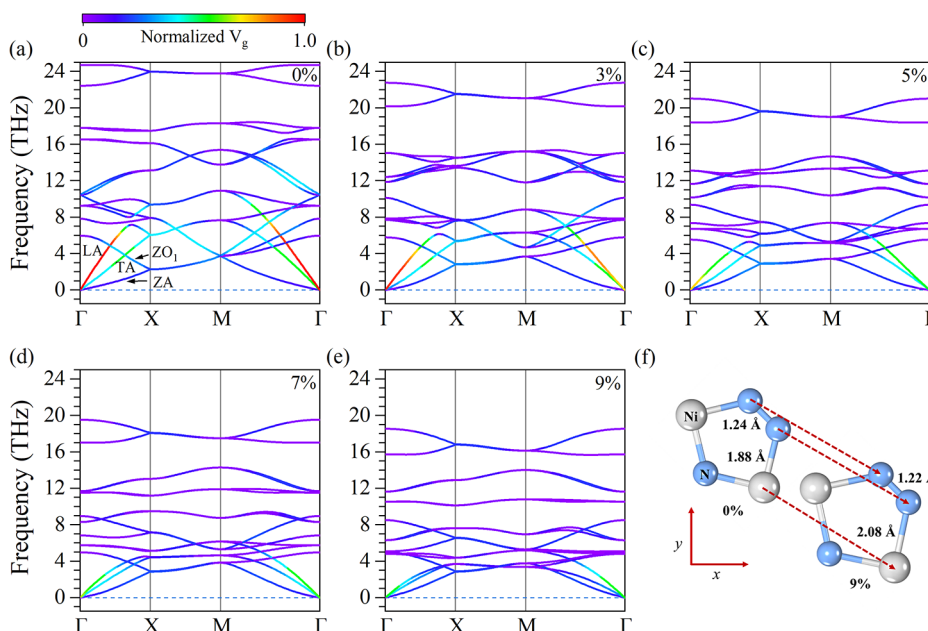


Figure 3. (a–e) Phonon spectra of penta-NiN₂ along the high symmetry path at 300 K under 0%, 3%, 5%, 7%, and 9% biaxial strain, respectively. Calculated group velocity values are projected as a color scale on the spectra, normalized by the calculated highest velocity value 10.97 km/s of the longitudinal acoustic (LA) mode of the unstrained penta-NiN₂ near the Γ point. (f) Ni–N and N–N bond lengths in pristine penta-NiN₂ and the 9% strained structure.

nonmonotonic behavior of previous studies on 2D materials.^{25,45} However, the trend changes into oscillating descent behavior once involving the temperature effect calculated by using SCPH theory. In previous studies on the lattice thermal conductivity of 2D materials, SCPH calculations were only applied to study the thermal conductivity of ferroelectric systems in different phases or improve the accuracy of calculations.^{20,51} This finding shows the importance of SCPH calculations in the study on the thermal conductivity of 2D materials. By calculating the three-phonon scattering rates, as shown in Figure 2c, one can see that the three-phonon scattering rates do not vary monotonously with strain, which contributes to the oscillatory decrease of the calculated κ_l^3 .

To further analyze the strain-tuned thermal transport behavior of penta-NiN₂, we calculate the phonon group velocities of this system at different strain conditions. The data projected on the phonon spectra are plotted in Figure 3a–e, which show that the normalized phonon group velocities of the longitudinal acoustic (LA), transverse acoustic (TA), and in-plane optical modes decrease with increased strain. Meanwhile, the vibrational frequencies of these modes also drop with the increase of strain. Moreover, to reveal the relationship between the change of strained structures and their phonon branches, the bond lengths of the Ni–N and N–N bonds of the structures with 9% strain and without strain are given in Figure 3f. According to the calculated vibrational density of states (VDOS) shown in Figure S5, the VDOS in the high frequency region contributed by N atoms becomes larger with the increased strain, suggesting weaker interaction between the Ni and N atoms, as is the case with 2D group-IV selenides.⁵² The weaker interaction between Ni and N atoms with larger Ni–N bond length results in the impediment to the propagation of in-plane vibrational modes. Compared with the in-plane modes, the reactions of flexural modes are relatively stable. Thus, flexural acoustic (ZA) and flexural optical (ZO) modes are slightly hardened with increasing strain. This phenomenon

indicates that the ZA and soft ZO modes may have significant influence on the κ_l^3 of penta-NiN₂ tuned by tensile strain.

In addition to the three-phonon scattering processes and phonon group velocities, the necessity of high order phonon scattering theory in the calculations of thermal conductivity has been demonstrated in previous studies.^{12,20} For more accurate results, we then discuss the effect of high order phonon scattering processes on the lattice thermal conductivity.

To study the effect of four-phonon scattering on the lattice thermal conductivity of penta-NiN₂, we recalculate the intrinsic lattice thermal conductivity κ_l^{3+4} based on four-phonon scattering theory. As shown in Figure 4, the calculated value is 11.67 W/mK at 300 K, corresponding to a reduction of 89.32% with respect to κ_l^3 (109.25 W/mK) without considering four-phonon scattering, as listed in Table 1,

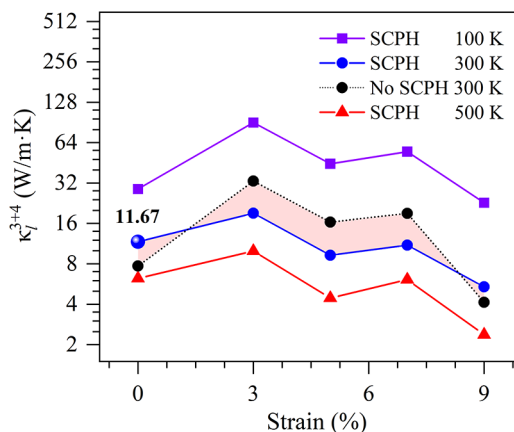


Figure 4. Variation of κ_l^{3+4} with strain calculated by considering the SCPH renormalization and four-phonon scattering at different temperatures (black dotted line and circles represent the thermal conductivity calculated without SCPH theory at 300 K).

Table 1. Percentage Decrease of κ_l^{3+4} with Respect to κ_l^3 at Different Temperatures and Strain Conditions

T (K)	0%	3%	5%	7%	9%
100	92.39%	75.94%	78.14%	65.87%	63.96%
300	89.32%	82.23%	83.88%	79.93%	79.93%
500	90.36%	85.36%	86.84%	83.89%	87.35%

indicating that the effect of four-phonon scattering processes dominates the lattice thermal conductivity. The underlying reason for this dramatic decrease of κ_l^{3+4} is related to the reflection symmetry of the planar penta-NiN₂ sheet, as discussed below.

Due to the reflection symmetry of planar 2D crystals, a selection rule exists in phonon–phonon scattering processes. When a 2D material in the *xy* plane maps the lattice into itself by the reflection about the *z*-axis, the *n*th IFC should satisfy the following relationship to guarantee the lattice potential to be invariant:⁵³

$$\Phi_{\alpha_1, \dots, \alpha_n}(i_{j_1}; \dots; i_{j_n}) = (-1)^m \Phi_{\alpha_1, \dots, \alpha_n}(i_{j_1}; \dots; i_{j_n}) \quad (2)$$

where $\Phi_{\alpha_1, \dots, \alpha_n}(i_{j_1}; \dots; i_{j_n})$ is the *n*th IFC of the system and *m* is the number of *z* components in the string of α . We can learn that, if *m* is an odd number, only when $\Phi_{\alpha_1, \dots, \alpha_n}(i_{j_1}; \dots; i_{j_n})$ equals zero can eq 2 be satisfied. This limitation prohibits all of the phonon–phonon scattering processes containing odd numbers of flexural modes. The low anharmonic scattering rates limited by this selection rule result in a high contribution ratio of ZA modes to the lattice thermal conductivity. Once the four-phonon scattering is induced in the calculations, the limitation of the selection rule will be weakened because of the huge increase of phonon scattering channels, thus leading to a lower lattice thermal conductivity.

To clearly show the effect of the selection rule on the lattice thermal conductivity of penta-NiN₂, we plot the cumulative κ_l^3 and κ_l^{3+4} with the spectral contributions in Figure 5. The spectral contributions to κ_l^3 shown in Figure 5c reveal that the

low frequency acoustic modes contribute most to the lattice thermal conductivity, which agrees with what Lindsay et al. reported in graphene.⁵³ Furthermore, Feng et al. reported significant influence of four-phonon scattering processes in graphene because more flexural modes are allowed to participate in the process of generating thermal resistance.¹² A similar phenomenon is observed in penta-NiN₂, as illustrated by the comparison between parts c and d of Figures 5. In addition, Figures S6 and S7 show that the four-phonon scattering rates of the ZA modes are 1 to 2 orders of magnitude higher than the three-phonon scattering rates of themselves, which confirms that the increased scattering rates of the ZA modes dominate the huge decrease of thermal conductivity.

The calculated results illustrate that the thermal conductivity remains negatively correlated with strain when including four-phonon scattering processes. The thermal response of penta-NiN₂ to strain still maintains the oscillating feature. Exactly, the calculated results of 3% and 7% strained penta-NiN₂ are higher than those of the 0% and 5% strained structures, plotted in Figure 4. As seen in Figure 5c and d, the spectral contributions of low frequency modes in structures with different strains exhibit different ratios, which can explain the trend of thermal conductivity numerically. These intriguing thermal responses can be attributed to the strain-tuned high order phonon scattering processes. To describe the four-phonon scattering processes in detail for revealing the origin of this unusual thermal phenomenon, we plot the four-phonon scattering rates of normal (N) and Umklapps (U) processes for low frequency phonon modes with respect to the reduced wave vector (Γ -X) in Figure 6.

The curves in Figure 6 show the four-phonon scattering rates of the N and U processes of each low frequency phonon branch with increased strain, where there are two types of phonon scattering processes with the same order of magnitude scattering rates. Moreover, the scattering rates of unstrained penta-NiN₂ are much higher than those of most strained

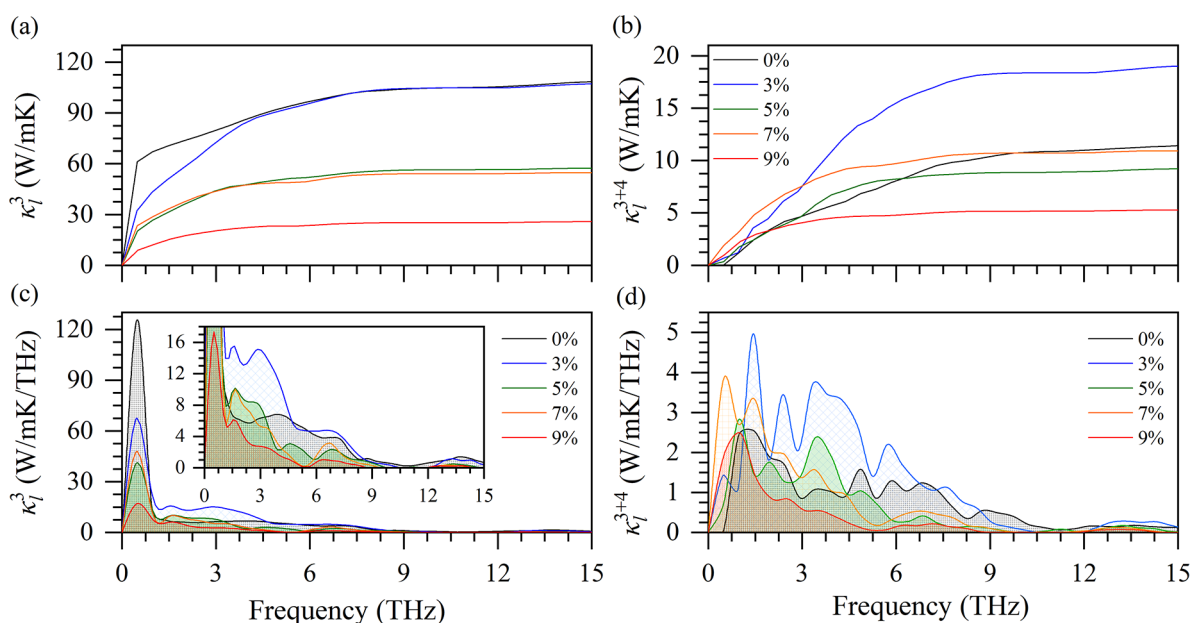


Figure 5. (a and b) Cumulative κ_l^3 and κ_l^{3+4} and (c and d) spectral contributions to κ_l^3 and κ_l^{3+4} of penta-NiN₂ at different biaxial strain conditions at 300 K, respectively. The inset in part c magnifies the spectral contributions to κ_l^3 under 18 W/mK/THz.

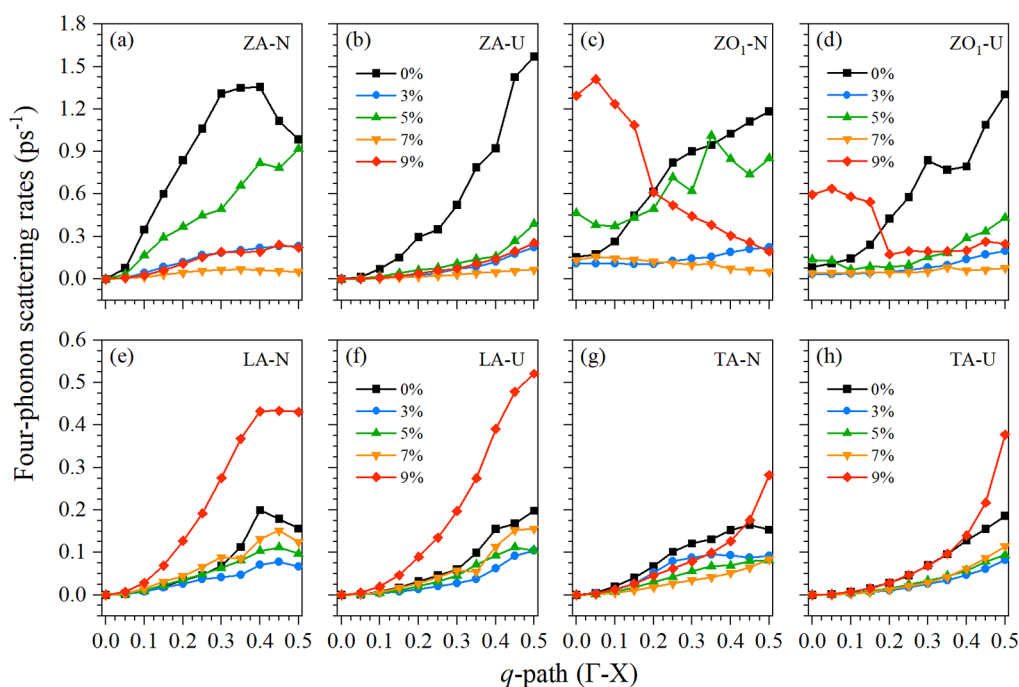


Figure 6. Four-phonon scattering rates of the N and U processes of the (a and b) ZA, (c and d) ZO_1 , (e and f) LA, and (g and h) TA branches with respect to the reduced wave vector (Γ -X) at 300 K, respectively.

structures, which is the origin of the huge decrease of the lattice thermal conductivity in unstrained penta-NiN₂. The calculated results indicate that the phonon modes in the unstrained structure may more easily satisfy the energy and momentum conservation of four-phonon scattering, which arises from the softening of in-plane phonon modes and the smaller phonon band gaps between the acoustic and optical modes. As shown in Figure S7, the strain-tuned three- and four-phonon scattering rates present a similarity in their change tendencies. However, the curve of the four-phonon scattering rates is smoother than that of the three-phonon scattering rates, which means that the high order scattering processes are less limited in momentum space. In addition, the scattering rates of the penta-NiN₂ sheet with 9% strain in the modes of the TA, LA, and ZO_1 branches are even higher than unstrained penta-NiN₂. The higher scattering rates of the TA and LA branches can be considered as the result of the ω_{LA}/ω_{TA} ratio approaching 1. Moreover, the change trend of the scattering rates in the ZO_1 branch of the 9% strained structure along the Γ -X path is contrary to those of other structures and contains a critical point at the reduced wave vector of 0.2. The phonon spectrum of the 9% strained structure shown in Figure 3e presents the absence of a phonon band gap between ZO_1 and other optical branches near the Γ point along the Γ -X path. As shown in Figure S8, the four-phonon scattering phase space (P4) of ZO_1 is relatively high, leading to anomalous scattering rates near the Γ point. Although the phonon band gap and symmetry selection rules are considered to have little effect on four-phonon scattering processes,^{54,55} the slight variety of strain-tuned four-phonon scattering can still significantly affect the lattice thermal conductivity of 2D materials. According to the above analysis, the strain-tuned phonon scattering rates combined with the decreased phonon group velocities together lead to the intriguing thermal response of penta-NiN₂ to biaxial tensile strain.

In summary, using the accurate theoretical methods based on BTE theory by considering a high order phonon scattering formalism and SCPH renormalization, we have studied the intrinsic and strain-tuned lattice thermal conductivity of the newly synthesized 2D pentagonal sheet, penta-NiN₂. The main conclusions can be summarized as the following: (1) Self-consistent phonon calculation has significant effects on the accuracy of the lattice thermal conductivity calculations and strain resistance of penta-NiN₂. (2) The intrinsic lattice thermal conductivity of penta-NiN₂ is only 11.67 W/mK at 300 K when both three- and four-phonon scattering are included, which is nearly 90% lower than that including only the three-phonon scattering formalism. (3) The lattice thermal conductivity of penta-NiN₂ exhibits an oscillatory drop with strain, which originates from the strain-tuned phonon group velocities and phonon-phonon scattering rates. (4) The strain-tuned three- and four-phonon scattering rates have a similar variation trend due to the softened in-plane vibration modes, stiff flexural modes, and gaps between phonon branches. Overall, our work makes an accurate analysis and illustrates the effects of SCPH renormalization and strain-tuned high order phonon scattering processes on the lattice thermal transport properties of penta-NiN₂, confirming that the calculations of SCPH renormalization and four-phonon scattering processes are necessary in the study on the lattice thermal conductivity of 2D planar pentagon-based materials.

■ ASSOCIATED CONTENT

SI Supporting Information

The Supporting Information is available free of charge at <https://pubs.acs.org/doi/10.1021/acs.jpcllett.2c01531>.

Additional data and figures, including the convergence test of the calculated thermal conductivity; thermal and mechanical stability; phonon spectra at different strain conditions; electronic band structures; vibrational

density of states; phonon scattering rates; and phase space (PDF)

AUTHOR INFORMATION

Corresponding Author

Qian Wang – School of Materials Science and Engineering, Center for Applied Physics and Technology, BKL-MEMD, Peking University, Beijing 100871, China; orcid.org/0000-0002-9766-4617; Email: qianwang2@pku.edu.cn

Authors

Chenxin Zhang – School of Materials Science and Engineering, Center for Applied Physics and Technology, BKL-MEMD, Peking University, Beijing 100871, China

Jie Sun – School of Materials Science and Engineering, Center for Applied Physics and Technology, BKL-MEMD, Peking University, Beijing 100871, China

Yiheng Shen – School of Materials Science and Engineering, Center for Applied Physics and Technology, BKL-MEMD, Peking University, Beijing 100871, China

Wei Kang – Center for Applied Physics and Technology, College of Engineering, Peking University, Beijing 100871, China

Complete contact information is available at: <https://pubs.acs.org/10.1021/acs.jpcllett.2c01531>

Notes

The authors declare no competing financial interest.

ACKNOWLEDGMENTS

This work is partially supported by grants from the National Key Research and Development Program of the Ministry of Science and Technology of China (2017YFA0205003) and the National Natural Science Foundation of China (NSFC-11974028). It is also supported by the High-Performance Computing Platform of Peking University, China.

REFERENCES

- (1) Lindsay, L.; Broido, D. A. Three-phonon phase space and lattice thermal conductivity in semiconductors. *J. Phys.: Condens. Matter* **2008**, *20* (16), 165209.
- (2) Lindsay, L.; Broido, D. A.; Mingo, N. Lattice thermal conductivity of single-walled carbon nanotubes: Beyond the relaxation time approximation and phonon-phonon scattering selection rules. *Phys. Rev. B* **2009**, *80* (12), 125407.
- (3) Nika, D. L.; Pokatilov, E. P.; Askerov, A. S.; Balandin, A. A. Phonon Thermal conduction in graphene: role of umklapp and edge roughness scattering. *Phys. Rev. B* **2009**, *79* (15), 155413.
- (4) Esfarjani, K.; Chen, G.; Stokes, H. T. Heat transport in silicon from first-principles calculations. *Phys. Rev. B* **2011**, *84* (8), 085204.
- (5) Turney, J. E.; Landry, E. S.; McGaughey, A. J. H.; Amon, C. H. Predicting phonon properties and thermal conductivity from anharmonic lattice dynamics calculations and molecular dynamics simulations. *Phys. Rev. B* **2009**, *79* (6), 064301.
- (6) Lindsay, L.; Broido, D. A.; Reinecke, T. L. Thermal conductivity and large isotope effect in GaN from first principles. *Phys. Rev. Lett.* **2012**, *109* (9), 095901.
- (7) Feng, T.; Ruan, X. Quantum mechanical prediction of four-phonon scattering rates and reduced thermal conductivity of solids. *Phys. Rev. B* **2016**, *93* (4), 045202.
- (8) Werthamer, N. R. Self-consistent phonon formulation of anharmonic lattice dynamics. *Phys. Rev. B* **1970**, *1* (2), 572–581.
- (9) Tadano, T.; Tsuneyuki, S. Self-consistent phonon calculations of lattice dynamical properties in cubic SrTiO₃ with first-principles anharmonic force constants. *Phys. Rev. B* **2015**, *92* (5), 054301.
- (10) Errea, I.; Calandra, M.; Mauri, F. Anharmonic free energies and phonon dispersions from the stochastic self-consistent harmonic approximation: Application to platinum and palladium hydrides. *Phys. Rev. B* **2014**, *89* (6), 064302.
- (11) Tadano, T.; Tsuneyuki, S. Quartic anharmonicity of rattlers and its effect on lattice thermal conductivity of clathrates from first principles. *Phys. Rev. Lett.* **2018**, *120* (10), 105901.
- (12) Feng, T.; Ruan, X. Four-phonon scattering reduces intrinsic thermal conductivity of graphene and the contributions from flexural phonons. *Phys. Rev. B* **2018**, *97* (4), 045202.
- (13) Kang, J. S.; Li, M.; Wu, H.; Nguyen, H.; Hu, Y. Experimental observation of high thermal conductivity in boron arsenide. *Science* **2018**, *361* (6402), 575–578.
- (14) Guo, S.-D. Biaxial strain tuned thermoelectric properties in monolayer PtSe₂. *J. Mater. Chem. C* **2016**, *4* (39), 9366–9374.
- (15) Zhang, J.; Liu, X.; Wen, Y.; Shi, L.; Chen, R.; Liu, H.; Shan, B. Titanium trisulfide monolayer as a potential thermoelectric material: A first-principles-based Boltzmann transport study. *ACS Appl. Mater. Interfaces* **2017**, *9* (3), 2509–2515.
- (16) Ma, J.; Meng, F.; He, J.; Jia, Y.; Li, W. Strain-induced ultrahigh electron mobility and thermoelectric figure of merit in monolayer α -Te. *ACS Appl. Mater. Interfaces* **2020**, *12* (39), 43901–43910.
- (17) Shi, W.; Ge, N.; Wang, X.; Wang, Z. High thermoelectric performance of Sb₂Si₂Te₆ monolayers. *J. Phys. Chem. C* **2021**, *125* (30), 16413–16419.
- (18) Gao, Z.; Wang, J.-S. Thermoelectric penta-silicene with a high room-temperature figure of merit. *ACS Appl. Mater. Interfaces* **2020**, *12* (12), 14298–14307.
- (19) Zhang, X.; Liu, C.; Tao, Y.; Li, Y.; Guo, Y.; Chen, Y.; Zeng, X. C.; Wang, J. High ZT 2D thermoelectrics by design: Strong interlayer vibration and complete band-extrema alignment. *Adv. Funct. Mater.* **2020**, *30* (22), 2001200.
- (20) Sun, J.; Zhang, C.; Yang, Z.; Shen, Y.; Hu, M.; Wang, Q. Four-phonon scattering effect and two-channel thermal transport in two-dimensional paraelectric SnSe. *ACS Appl. Mater. Interfaces* **2022**, *14* (9), 11493–11499.
- (21) Shen, Y.; Wang, Q. Pentagon-based 2D materials: Classification, properties and applications. *Phys. Rep.* **2022**, *964*, 1–42.
- (22) Zhang, S.; Zhou, J.; Wang, Q.; Chen, X.; Kawazoe, Y.; Jena, P. Penta-graphene: A new carbon allotrope. *Proc. Natl. Acad. Sci. U. S. A.* **2015**, *112* (8), 2372–2377.
- (23) Wang, F. Q.; Yu, J.; Wang, Q.; Kawazoe, Y.; Jena, P. Lattice thermal conductivity of penta-graphene. *Carbon* **2016**, *105*, 424–429.
- (24) Wang, F. Q.; Liu, J.; Li, X.; Wang, Q.; Kawazoe, Y. Weak interlayer dependence of lattice thermal conductivity on stacking thickness of penta-graphene. *Appl. Phys. Lett.* **2017**, *111* (19), 192102.
- (25) Liu, H.; Qin, G.; Lin, Y.; Hu, M. Disparate strain dependent thermal conductivity of two-dimensional penta-structures. *Nano Lett.* **2016**, *16* (6), 3831–3842.
- (26) Bykov, M.; Bykova, E.; Ponomareva, A. V.; Tasnádi, F.; Chariton, S.; Prakupenka, V. B.; Glazyrin, K.; Smith, J. S.; Mahmood, M. F.; Abrikosov, I. A.; Goncharov, A. F. Realization of an ideal Cairo tessellation in nickel diazenide NiN₂: High-pressure route to pentagonal 2D materials. *ACS Nano* **2021**, *15* (8), 13539–13546.
- (27) Yuan, J.-H.; Song, Y.-Q.; Chen, Q.; Xue, K.-H.; Miao, X.-S. Single-layer planar penta-X₂N₄ (X = Ni, Pd and Pt) as direct-bandgap semiconductors from first principle calculations. *Appl. Surf. Sci.* **2019**, *469*, 456–462.
- (28) Blöchl, P. E. Projector augmented-wave method. *Phys. Rev. B* **1994**, *50* (24), 17953–17979.
- (29) Kresse, G.; Joubert, D. From ultrasoft pseudopotentials to the projector augmented-wave method. *Phys. Rev. B* **1999**, *59* (3), 1758–1775.
- (30) Kresse, G.; Furthmüller, J. Efficient iterative schemes for ab initio total-energy calculations using a plane-wave basis set. *Phys. Rev. B* **1996**, *54* (16), 11169–11186.
- (31) Perdew, J. P.; Burke, K.; Ernzerhof, M. Generalized gradient approximation made simple. *Phys. Rev. Lett.* **1996**, *77* (18), 3865–3868.

- (32) Hu, Y. F.; Storey, C. Efficient generalized conjugate gradient algorithms, part 2: Implementation. *J. Optim. Theory Appl.* **1991**, *69* (1), 139–152.
- (33) Heyd, J.; Scuseria, G. E.; Ernzerhof, M. Hybrid functionals based on a screened Coulomb potential. *J. Chem. Phys.* **2003**, *118* (18), 8207–8215.
- (34) Heyd, J.; Scuseria, G. E.; Ernzerhof, M. Erratum: “Hybrid functionals based on a screened Coulomb potential” [*J. Chem. Phys.* **2006**, *124* (21), 219906]. *J. Chem. Phys.* **2006**, *124* (21), 219906.
- (35) Omini, M.; Sparavigna, A. An iterative approach to the phonon Boltzmann equation in the theory of thermal conductivity. *Phys. B Condens. Matter* **1995**, *212* (2), 101–112.
- (36) Han, Z.; Yang, X.; Li, W.; Feng, T.; Ruan, X. FourPhonon: An extension module to ShengBTE for computing four-phonon scattering rates and thermal conductivity. *Comput. Phys. Commun.* **2022**, *270*, 108179.
- (37) Togo, A.; Tanaka, I. First principles phonon calculations in materials science. *Scr. Mater.* **2015**, *108*, 1–5.
- (38) Eriksson, F.; Fransson, E.; Erhart, P. The Hiphive package for the extraction of high-order force constants by machine learning. *Adv. Theory Simul.* **2019**, *2* (5), 1800184.
- (39) Fransson, E.; Eriksson, F.; Erhart, P. Efficient construction of linear models in materials modeling and applications to force constant expansions. *Npj Comput. Mater.* **2020**, *6* (1), 1–11.
- (40) Wu, X.; Varshney, V.; Lee, J.; Pang, Y.; Roy, A. K.; Luo, T. How to characterize thermal transport capability of 2D materials fairly? – Sheet Thermal conductance and the choice of thickness. *Chem. Phys. Lett.* **2017**, *669*, 233–237.
- (41) Sun, Z.; Yuan, K.; Zhang, X.; Qin, G.; Gong, X.; Tang, D. Disparate strain response of the thermal transport properties of bilayer penta-graphene as compared to that of monolayer penta-graphene. *Phys. Chem. Chem. Phys.* **2019**, *21* (28), 15647–15655.
- (42) Born, M.; Huang, K.; Lax, M. Dynamical theory of crystal lattices. *Am. J. Phys.* **1955**, *23*, 474–474.
- (43) Ding, Y.; Wang, Y. Density functional theory study of the silicene-like SiX and XSi₃ (X = B, C, N, Al, P) honeycomb lattices: The various buckled structures and versatile electronic properties. *J. Phys. Chem. C* **2013**, *117* (35), 18266–18278.
- (44) Mouhat, F.; Coudert, F.-X. Necessary and sufficient elastic stability conditions in various crystal systems. *Phys. Rev. B* **2014**, *90* (22), 224104.
- (45) Hu, M.; Zhang, X.; Poulidakos, D. Anomalous thermal response of silicene to uniaxial stretching. *Phys. Rev. B* **2013**, *87* (19), 195417.
- (46) Mortazavi, B.; Zhuang, X.; Rabczuk, T.; Shapeev, A. V. Outstanding thermal conductivity and mechanical properties in the direct gap semiconducting penta-NiN₂ monolayer confirmed by first-principles. *Phys. E Low-Dimens. Syst. Nanostructures* **2022**, *140*, 115221.
- (47) Mortazavi, B.; Podryabinkin, E. V.; Novikov, I. S.; Rabczuk, T.; Zhuang, X.; Shapeev, A. V. Accelerating first-principles estimation of thermal conductivity by machine-learning interatomic potentials: A MTP/ShengBTE solution. *Comput. Phys. Commun.* **2021**, *258*, 107583.
- (48) Xu, W.; Zhang, G.; Li, B. Thermal conductivity of penta-graphene from molecular dynamics study. *J. Chem. Phys.* **2015**, *143* (15), 154703.
- (49) Gu, X.; Wei, Y.; Yin, X.; Li, B.; Yang, R. Colloquium: Phononic thermal properties of two-dimensional materials. *Rev. Mod. Phys.* **2018**, *90* (4), 041002.
- (50) Dai, Z.; Liu, L.; Zhang, Z. Strain engineering of 2D materials: Issues and opportunities at the interface. *Adv. Mater.* **2019**, *31* (45), 1805417.
- (51) Pandit, A.; Hamad, B. The effect of finite-temperature and anharmonic lattice dynamics on the thermal conductivity of ZrS₂ monolayer: Self-consistent phonon calculations. *J. Phys.: Condens. Matter* **2021**, *33* (42), 425405.
- (52) Liu, P.-F.; Bo, T.; Xu, J.; Yin, W.; Zhang, J.; Wang, F.; Eriksson, O.; Wang, B.-T. First-principles calculations of the ultralow thermal conductivity in two-dimensional group-IV selenides. *Phys. Rev. B* **2018**, *98* (23), 235426.
- (53) Lindsay, L.; Broido, D. A.; Mingo, N. Flexural phonons and thermal transport in graphene. *Phys. Rev. B* **2010**, *82* (11), 115427.
- (54) Feng, T.; Lindsay, L.; Ruan, X. Four-phonon scattering significantly reduces intrinsic thermal conductivity of solids. *Phys. Rev. B* **2017**, *96* (16), 161201.
- (55) Ravichandran, N. K.; Broido, D. Phonon-phonon interactions in strongly bonded solids: Selection rules and higher-order processes. *Phys. Rev. X* **2020**, *10* (2), 021063.